Improving magnetic resonance spectroscopy in the brainstem periaqueductal gray using spectral registration

Sirucek, Laura ; Zoelch, Niklaus ; Schweinhardt, Petra

Abstract: Purpose: Functional understanding of the periaqueductal gray (PAG), a clinically relevant brainstem region, can be advanced using ^{1}H-MRS. However, the PAG's small size and high levels of physiological noise are methodologically challenging. This study aimed to (1) improve ^{1}H-MRS quality in the PAG using spectral registration for frequency and phase error correction; (2) investigate whether spectral registration is particularly useful in cases of greater head motion; and (3) examine metabolite quantification using literature-based or individual-based water relaxation times. Methods: Spectra were acquired in 33 healthy volunteers (50.1 years, SD = 17.19, 18 females) on a 3 T Philipps MR system using a point-resolved spectroscopy (PRESS) sequence optimized with very selective saturation pulses (OVERPRESS) and voxel-based flip angle calibration (effective volume of interest size: 8.8 × 10.2 × 12.2 mm^3). Spectra were fitted using LCModel and SNR, NAA peak linewidths and Cramér-Rao lower bounds (CRLBs) were measured after spectral registration and after minimal frequency alignment. Results: Spectral registration improved SNR by 5% ($p = 0.026$, median value post-correction: 18.0) and spectral linewidth by 23% ($p < 0.001$, 4.3 Hz), and reduced the metabolites' CRLBs by 1% to 15% ($p < 0.026$). Correlational analyses revealed smaller SNR improvements with greater head motion ($p = 0.010$) recorded using a markerless motion tracking system. Higher metabolite concentrations were detected using individual-based compared to literature-based water relaxation times ($p < 0.001$). Conclusion: This study demonstrates high-quality ^{1}H-MRS acquisition in the PAG using spectral registration. This shows promise for future ^{1}H-MRS studies in the PAG and possibly other clinically relevant brain regions with similar methodological challenges.

DOI: https://doi.org/10.1002/mrm.29832

Received: 31 March 2023 | Revised: 8 July 2023 | Accepted: 31 July 2023

DOI: 10.1002/mrm.29832

Magnetic Resonance in Medicine

TECHNICAL NOTE

Improving magnetic resonance spectroscopy in the brainstem periaqueductal gray using spectral registration

Laura Sirucek[1,2] | **Niklaus Zoelch**[3,4] | **Petra Schweinhardt**[1,2]

[1]Department of Chiropractic Medicine, Integrative Spinal Research Group, Balgrist University Hospital, University of Zurich, Zurich, Switzerland

[2]Neuroscience Center Zurich, University of Zurich, Zurich, Switzerland

[3]Department of Forensic Medicine and Imaging, Institute of Forensic Medicine, University of Zurich, Zurich, Switzerland

[4] Department of Psychiatry, Psychotherapy, and Psychosomatics, Psychiatric University Hospital Zurich, University of Zurich, Zurich, Switzerland

Correspondence
Laura Sirucek, Department of Chiropractic Medicine, Integrative Spinal Research Group, Balgrist Campus, Lengghalde 5 8008 Zurich, Switzerland.
Email: laura.sirucek@balgrist.ch

Funding information
University of Zurich, Grant/Award Number: Clinical Research Priority Program "Pain"

Abstract

Purpose: Functional understanding of the periaqueductal gray (PAG), a clinically relevant brainstem region, can be advanced using ^{1}H-MRS. However, the PAG's small size and high levels of physiological noise are methodologically challenging. This study aimed to (1) improve ^{1}H-MRS quality in the PAG using spectral registration for frequency and phase error correction; (2) investigate whether spectral registration is particularly useful in cases of greater head motion; and (3) examine metabolite quantification using literature-based or individual-based water relaxation times.

Methods: Spectra were acquired in 33 healthy volunteers (50.1 years, SD = 17.19, 18 females) on a 3 T Philipps MR system using a point-resolved spectroscopy (PRESS) sequence optimized with very selective saturation pulses (OVERPRESS) and voxel-based flip angle calibration (effective volume of interest size: $8.8 \times 10.2 \times 12.2\,mm^3$). Spectra were fitted using LCModel and SNR, NAA peak linewidths and Cramér-Rao lower bounds (CRLBs) were measured after spectral registration and after minimal frequency alignment.

Results: Spectral registration improved SNR by 5% ($p = 0.026$, median value post-correction: 18.0) and spectral linewidth by 23% ($p < 0.001$, 4.3 Hz), and reduced the metabolites' CRLBs by 1% to 15% ($p < 0.026$). Correlational analyses revealed smaller SNR improvements with greater head motion ($p = 0.010$) recorded using a markerless motion tracking system. Higher metabolite concentrations were detected using individual-based compared to literature-based water relaxation times ($p < 0.001$).

Conclusion: This study demonstrates high-quality ^{1}H-MRS acquisition in the PAG using spectral registration. This shows promise for future ^{1}H-MRS studies in the PAG and possibly other clinically relevant brain regions with similar methodological challenges.

KEYWORDS

brainstem, head motion, magnetic resonance spectroscopy, postprocessing, relaxation time, small volume

1 | INTRODUCTION

The periaqueductal gray (PAG) is a brainstem region with multiple pivotal functions for the human organism including the coordination of cardiovascular, respiratory, motor, and pain modulatory reactions to stress.[1] Various pathological conditions present with changes in PAG function. For instance, altered PAG functional connectivity has been observed in neurodegenerative diseases,[2,3] migraine,[4,5] headache,[6] fibromyalgia,[7–9] neuropathic pain,[10] and chronic low back pain.[11] A more complete understanding of PAG function in health and disease can be gained by examining the PAG's neurochemical properties. ^{1}H-MRS offers a non-invasive method to obtain in vivo neurochemical information about human brain tissue.

In the PAG, ^{1}H-MRS has been investigated in patients with chronic migraine,[12,13] chronic daily headaches,[14] and chronic whiplash injury.[15] Yet, the number of ^{1}H-MRS studies in the PAG is limited, which may be because of several difficulties associated with ^{1}H-MRS acquisition in this region: first, the PAG is a small structure of ~4 to 5 mm diameter and 14 mm length,[16] that is $\sim 5 \times 5 \times 14\,mm^3$ (anterior-posterior × left-right × foot-head). Second, the PAG is prone to physiological noise because of its proximity to pulsating anatomical structures, such as major arteries and CSF-filled spaces.[17] The existing PAG ^{1}H-MRS studies used different approaches to address these challenges. Lai and colleagues[12] used a long TE of 144 ms, which produces a better baseline and allows a more stable detection of the main metabolites Cr, Cho, and NAA.[18] However, various neurobiologically relevant metabolites, for example, myo-inositol (mI) or glutamate (Glu), require shorter TEs to be detected. Another option is to sacrifice regional specificity by using volume of interest (VOI) sizes lager than the PAG itself (e.g., $20 \times 20 \times 20\,mm^3$)[13,14] because the SNR increases proportionally to VOI size.[19] Smaller VOIs require longer acquisition times to achieve sufficient SNR, which might in turn impair the spectral quality because of increasing frequency drifts over time and a higher risk for head motion inducing additional frequency and phase errors.[20,21] Promising tools to correct for frequency and phase drifts or errors are offered by advanced postprocessing techniques such as spectral registration.[20]

In this study, the aim was to record high-quality ^{1}H-MR spectra in a $8.8 \times 10.2 \times 12.2\,mm^3$ VOI covering the PAG of healthy volunteers using a point-resolved spectroscopy sequence (PRESS)[22,23] optimized with very selective saturation pulses (OVERPRESS)[24–26] and voxel-based flip angle calibration[27,28] combined with spectral registration.[20] The spectral quality was compared to the spectral quality achieved with minimal frequency alignment, which is, using the unsuppressed water peak of multiple interleaved spectra. In addition, it was investigated whether spectral registration was particularly useful in cases of greater head motion measured with a markerless motion tracking system.[29] Last, because tissue-specific water T_1 and T_2 relaxation times vary across different brain regions[30–32] and standard literature-based values might not generalize to the PAG, differences in metabolite concentrations using literature-based or individual-based water relaxation times were examined. The data presented in this manuscript are part of a larger study investigating differences in PAG spectra between pain-free volunteers and chronic low back pain patients.

2 | METHODS

2.1 | Participants

Thirty-five healthy volunteers were recruited via online advertisements and oral communication. The participants were age- and sex-matched to a cohort of chronic low back pain patients as part of a larger study (Clinical Research Priority Program "Pain," https://www.crpp-pain.uzh.ch/en.html). The patient cohort data are not part of the present research question, and therefore, not discussed. Inclusion criteria were between 18 and 80 years of age and free of low back pain lasting longer than three consecutive days during the last year. Exclusion criteria comprised any major medical or psychiatric condition, pregnancy, inability to follow study instructions, and any contraindication to MRI. The study was approved by the local ethics committee "Kantonale Ethikkommission Zürich" (no. 2019–00136; clinicaltrials.gov: NCT04433299) and was performed according to the guidelines of the Declaration of Helsinki (2013). Written informed consent was obtained from all participants before the start of the experiment.

2.2 | Study Design Overview

The larger study comprised three experimental sessions of ~3 h each. The first two sessions included clinical, neurophysiological, and psychophysical assessments. During the third session, participants underwent two MR measurements, one ^{1}H-MRS scan, and one resting state functional MRI scan with a break of 1 h in between. All scans were performed after 12 PM. Only the ^{1}H-MRS data are subject of the present study.

2.3 | MRS

Technical details of the ^{1}H-MRS acquisition, postprocessing, and metabolite quantification are listed in Table S1. The following sections provide a brief overview of the applied methods.

2.3.1 | Acquisition

^{1}H-MRS was acquired on a 3 T MR system using a 32-channel receive-only phased-array head coil (Philips Healthcare). Before ^{1}H-MRS acquisition, high-resolution (1 mm^3 isotropic) anatomical T_1-weighted images were obtained. Based on the 3D T_1 images, the VOI was placed to cover the PAG according to anatomical landmarks by the same examiner (L.S.) for all participants (Figure 1). Spectra were localized using a water-suppressed single-voxel PRESS sequence[22,23] (TR: 2500 ms, TE: 33 ms, number of signals averaged: 512 divided into 8 blocks of 64) optimized with six very selective saturation (VSS) pulses (OVERPRESS)[24–26] to minimize errors in chemical-shift displacement and to achieve consistent localization volumes across all metabolites of interest (Figure 1), and with voxel-based flip angle calibration[27,28] to achieve an optimal flip angle within the VOI. Accounting for the VSS pulses, the resulting VOI size was $8.8 \times 10.2 \times 12.2$ mm^3 = 1.1 mL. For each individual, two water signals were acquired: one for eddy-current correction and literature-based water referencing obtained from interleaved water unsuppressed spectra (one before each of the 8 blocks) during the ^{1}H-MRS acquisition in the PAG (WR-shortTR) and one for an individual-based water referencing approach (see 2.3.3 Metabolite quantification), where a fully relaxed water signal was estimated from a separate water reference scan after the ^{1}H-MRS acquisition in the PAG within the same VOI with a TR of 10 000 ms (WR-longTR) and varying TEs (33/66/107/165/261/600 ms). The 3D T_1 and ^{1}H-MRS acquisition in the PAG took 7 min 32 s and 23 min 20 s, respectively.

2.3.2 | Postprocessing

For the approach with spectral registration, frequency alignment was performed using spectral registration in the time domain (adopted from Near et al. and Simpson et al.).[20,33] For that, the data was filtered with a 2 Hz Gaussian filter. Only the first 500 ms were used for alignment and the single averages were aligned to the median of all averages. Without spectral registration, minimal frequency alignment was achieved by eddy-current correction,[34] that is, eddy-current correcting the 64 averages of each block using the unsuppressed water scan (WR-shortTR) acquired before the respective block.

For both approaches, the postprocessed spectra were visually checked for artifacts. Spectra with artifacts were excluded from further analyses, as well as spectra presenting with insufficient quality,[28] that is, with a FWHM value of the unsuppressed water peak (FWHM H_2O; shim quality indicator) above 2.5 median absolute deviation (MAD)[35] of the group median or with an SNR (as obtained from LCModel) below 2.5 MAD of the group median.

2.3.3 | Metabolite quantification

All spectra were analyzed using LCModel (6.3).[36] Metabolite concentrations are reported as ratios to the unsuppressed water signal and reflect an estimation of metabolite concentration in moles per kg of tissue water excluding water within CSF. The fully relaxed water signal was estimated in two ways: (1) literature-based, using the unsuppressed water signal from the WR-shortTR scans and literature values to correct relaxation attenuation; and (2) individual-based, using the TE series acquired with the WR-longTR scan. Varying TEs allow to estimate the T_2 relaxation time of water within the VOI and therewith, to obtain a subject-specific approximation of the fully relaxed water signal.[37] Next to being independent of literature-based tissue-specific T_1 and T_2 relaxation times, this approach is also less reliant on correct segmentation of gray matter (GM), white matter (WM) and CSF compared to the literature-based approach.

2.3.4 | Motion tracking

Head motion was measured in 25 participants using the markerless motion tracking system Tracoline TCL3 with the TracSuite software 3.1.9 (TracInnovations) used for retrospective motion correction of positron emission tomography scans[38,39] and prospective real-time motion correction of MRI scans.[39,40] A more detailed description of the Tracoline system is provided in Figure S1. A representative recording of a participant's absolute 3D motion is displayed in Figure 2. From this 3D motion recording, two 3D motion parameters were calculated (Figure 2): (1) the 3D motion SD (3D SD) during the ^{1}H-MRS scan, representing an estimate for head motion variability; and (2) the difference in 3D motion (3D DIFF) from the beginning to the end of the ^{1}H-MRS scan, representing an estimate of the mean head displacement.

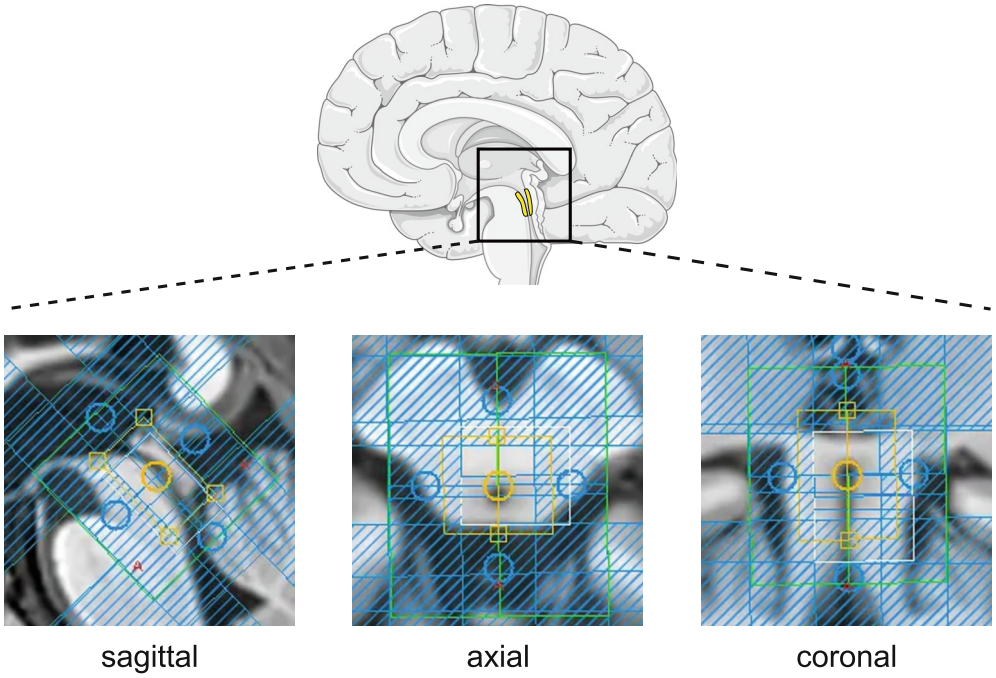

FIGURE 1 Volume of interest (VOI) placement over the brainstem periaqueductal gray. The yellow box depicts the VOI's nominal size ($11 \times 15 \times 18\ mm^3$ [anterior-posterior × left-right × foot-head]). The blue-shaded areas depict the six very selective saturation (VSS) bands used to minimize errors in chemical-shift displacement and to achieve consistent localization volumes across all metabolites of interest. The unshaded area within the yellow box depicts the final VOI size ($8.8 \times 10.2 \times 12.2\ mm^3$) accounting for the VSS bands. The schematic brain was adapted from Servier Medical Art (smart.servier.com).

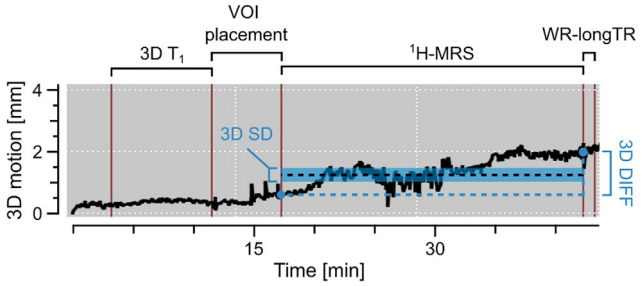

FIGURE 2 Representative absolute 3D motion recording. The two calculated 3D motion parameters are visually represented in blue: 3D motion SD (3D SD) as estimate for head motion variability and (2) the difference in 3D motion (3D DIFF) as estimate of the mean head displacement. Figure S1 describes how mean head displacement is related to the conventional six-parameter description of head motion, that is, x-, y-, and z- translations and rotations. The beginning and the end of the ^{1}H-MRS acquisition in the periaqueductal gray was manually labeled during the scan (red lines) within the TracSuite software. 3D T_1, anatomical T_1-weighted scan; VOI, volume of interest; WR-longTR, water reference scan with a long repetition time.

2.4 | Statistical analysis

All statistical analyses were performed using RStudio for Mac (2022.12.0 + 353). Statistical significance was set at $\alpha = 0.05$ with a false discovery rate (FDR) correction per tested research question. The number of corrected tests per research question is indicated as N-FDR.

Normal distribution was assessed via inspection of histograms and QQ-plots. Because the majority of investigated outcome measures were not normally distributed, all values are reported as median (interquartile range) and all statistical analyses were performed using non-parametric tests.

SNR and FWHM of the NAA peak (FWHM NAA; as obtained from LCModel; postprocessing quality indicator), as well as absolute Cramér-Rao lower bounds (CRLB) (relative CRLBs corrected for the metabolite concentration)[41] for the metabolites tCr (Cr + phosphocreatine), tCho (glycerophosphocholine + phosphocholine), tmI (mI + glycine), tNAA (NAA + N-acetylaspartylglutamate), pooled levels of Glu + Glutamine (Glx), and GABA, were compared between spectra processed with spectral registration and spectra processed without spectral registration using Pratt signed-rank tests (an alternative for Wilcoxon signed-rank tests accounting for ties)[42] (N-FDR = 8).

To investigate whether spectral registration was particularly useful in cases of greater head motion, relative improvements in SNR and FWHM NAA were correlated with head motion variability (3D SD) and mean head displacement (3D DIFF) using Spearman correlations (N-FDR = 4).

Metabolite concentrations of tCr, tCho, tmI, tNAA, Glx, and GABA were compared between the literature-based and the individual-based metabolite quantification approach, that is, using the water signal from the WR-shortTR scan and using the water signal from the WR-longTR scan, respectively, using Pratt signed-rank tests (N-FDR = 6).

For Pratt signed-rank tests, effect sizes are reported as r (small effect: 0.1 to <0.3, medium effect: 0.3 to <0.5, large effect: ≥0.5).[43]

3 | RESULTS

3.1 | Participant demographics

Of the 35 recruited participants, one was excluded because of a suspected neurological disorder and one discontinued the scanning session because of discomfort. This resulted in a sample of 33 participants (mean age of 50.1 years, SD = 17.19, 18 females) in whom ^{1}H-MRS was performed.

For spectra processed with spectral registration and spectra processed without spectral registration, visual inspection led to the exclusion of the same three participants (Figure S2). No participant presented with FWHM H_2O above or SNR values below 2.5 MAD of the sample median.

3.2 | Improved spectral quality with spectral registration

A representative single spectrum and overlaid single spectra together with the group average for both postprocessing approaches are shown in Figure 3. The FWHM H_2O reflecting the quality of the shim was 5.4 Hz (4.88–5.62) (Figure 4A).

Spectral registration significantly improved the SNR (median improvement: 4.8%, $Z = 2.26$, $p = 0.026$, $r = 0.41$), FWHM NAA (22.6%, $Z = -4.72$, $p < 0.001$, $r = 0.86$), and absolute CRLBs of all investigated metabolites (1.3%–14.7%, $Z < -2.22$, $p < 0.026$, $r > 0.41$) of the acquired spectra (Table 1, Figure 4B). Given the low SNR of the single averages, spectral registration required a sufficiently large residual water peak (ratio to NAA peak: 8.8 [8.40–9.60]).

3.2.1 | Less improvement in spectral quality with greater head motion

On average, participants showed a head motion variability (3D SD) of 0.5 mm (0.32–0.73) and a mean head displacement (3D DIFF) of 1.7 mm (0.62–2.64) during the ^{1}H-MRS scan.

Greater mean head displacement (3D DIFF; $\rho = -0.58$; $p = 0.010$), but not head motion variability (3D SD; $\rho = -0.31$; $p = 0.259$) was associated with less relative improvement in SNR (Figure S3). Relative improvement in FWHM NAA was not associated with head motion measures ($\rho < 0.3$; $p > 0.259$).

3.3 | Higher metabolite concentrations using individual-based quantification approach

Metabolite quantification using the subject-specific water signal from the WR-longTR scan, that is, the individual-based quantification approach, yielded higher concentrations for all investigated metabolites ($Z > 4.29$, $p < 0.001$, $r > 0.78$) compared to the literature-based approach using the water signal from the WR-longTR scan (Table 1, Figure S4). T_2 relaxation times estimated via the TE series in the WR-longTR scan were 81.25 ms (77.75–84.2).

4 | DISCUSSION AND CONCLUSIONS

This study aimed to record high-quality ^{1}H-MR spectra with optimized regional specificity in the brainstem PAG. Spectral registration[20] was used to address the challenge of increased frequency drifts and phase errors during the prolonged ^{1}H-MRS acquisition needed for the small VOI size of $8.8 \times 10.2 \times 12.2\,mm^3$. Using spectral registration, all quality measures of the acquired spectra improved, resulting in high spectral quality in the methodologically challenging PAG.

Compared to previous PAG ^{1}H-MRS studies,[12–15] this study's approach allowed higher regional specificity together with quantification of neurobiologically relevant metabolites detected at short TEs such as Glx. Because these previous studies did not report spectral quality measures, a direct quality comparison is not possible. However, the spectral quality achieved here is comparable or even superior to studies, which examined other brainstem VOIs of larger size[44–49] and superior to one study with a brainstem VOI of similar size.[50] Spectral registration improving SNR and NAA linewidth by ~5% and 23%, respectively, is relevant for several reasons. First, using spectral registration, VOI size could be decreased by 5% or acquisition time by 10%. This moderate effect is complemented by the more pronounced linewidth improvement. Narrower linewidths benefit metabolite detection independent of SNR, for example, it has been shown that at constant SNR, broader linewidths decrease metabolite quantification accuracy.[51] This is most likely because of hampered peak fitting and differentiation of overlapping peaks, supported by observations of larger absolute CRLBs with broader

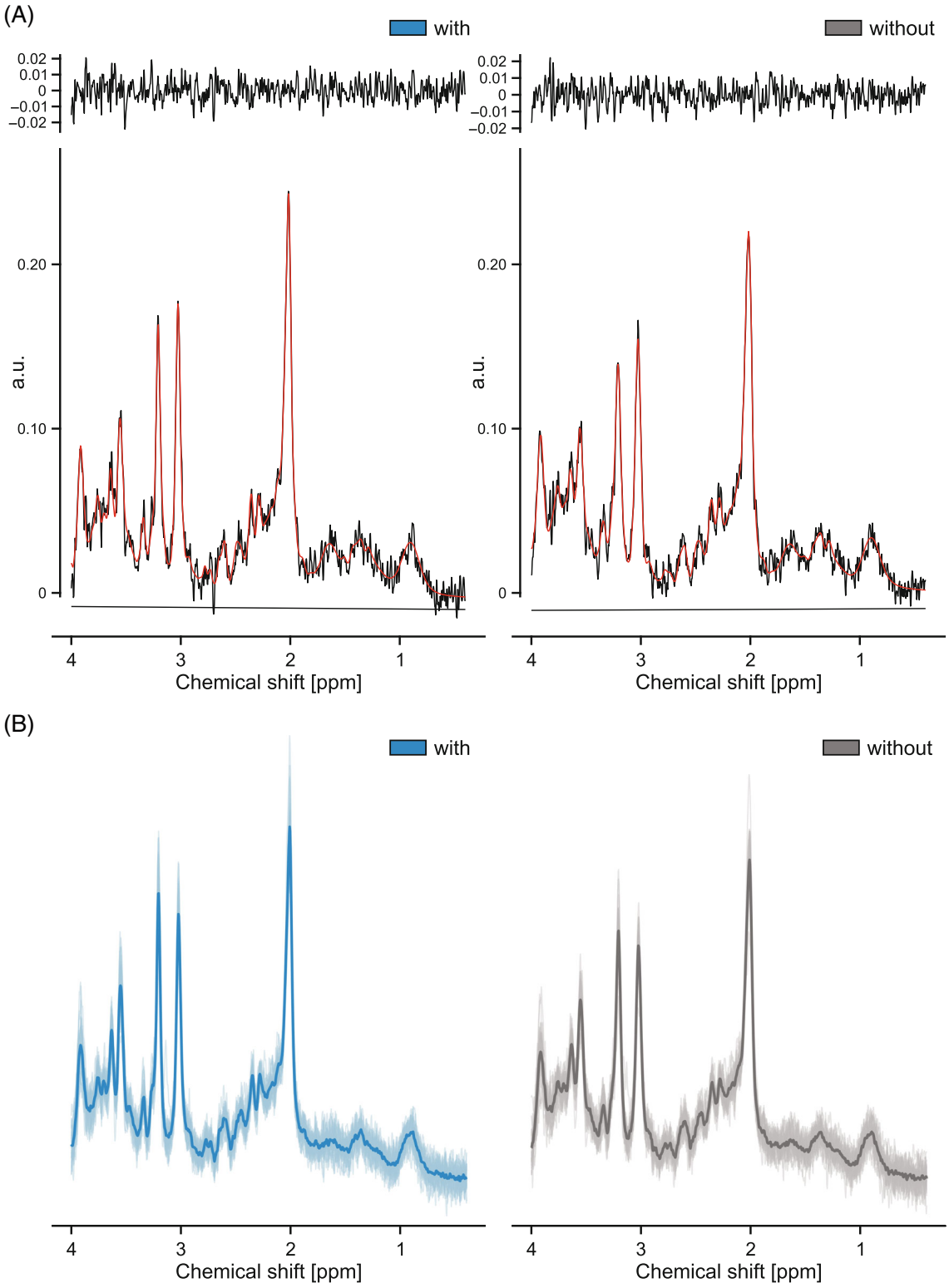

FIGURE 3 Spectra processed with and without spectral registration. Representative single spectra and overlaid LCModel fits (red line) shown in (A) are from the same individual who showed an SNR of 18, that is, the group median, in both postprocessing approaches and an NAA linewidth improvement from 6.9 Hz without spectral registration (right panel) to 4.9 Hz with spectral registration (left panel) (29.6%). (B) Overlaid single spectra together with the group average (bold) for spectra processed with (blue) and spectra processed without (gray) spectral registration. Spectra were acquired using a PRESS sequence optimized with very selective saturation pulses (OVERPRESS) and voxel-based flip angle calibration (TR: 2500 ms, TE: 33 ms, number of signals averaged: 512 divided into 8 blocks of 64, volume of interest size: $8.8 \times 10.2 \times 12.2\,\text{mm}^3 = 1.1\,\text{mL}$).

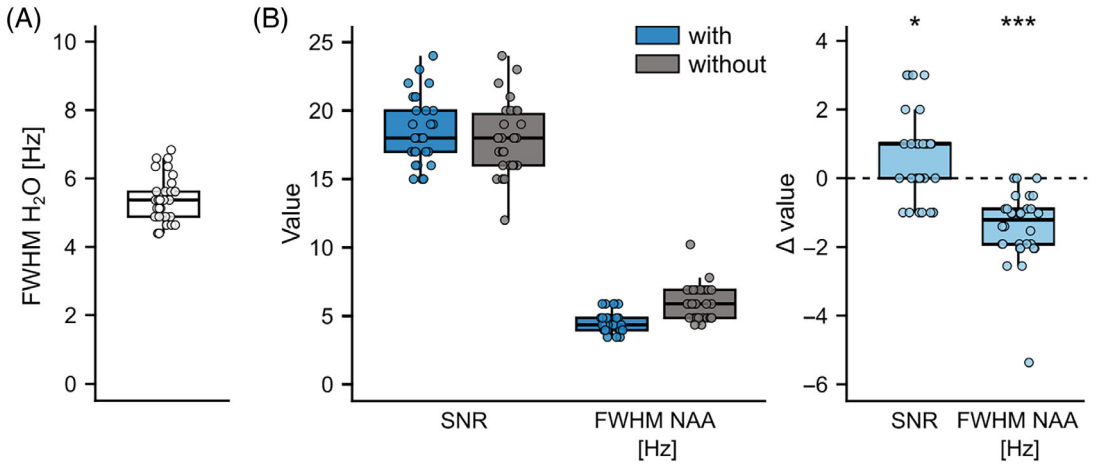

FIGURE 4 Improved spectral quality with spectral registration. FWHM values of the water peak (FWHM H_2O) (A) reflect the quality of the shim and apply to both postprocessing approaches. Differences (Δ) in SNR and FWHM of the NAA peak (FWHM NAA) were calculated by subtracting the values obtained without spectral registration from the values obtained with spectral registration. An improvement using spectral registration is reflected in positive differences for SNR and in negative differences for FWHM NAA. *$p < 0.05$, ***$p < 0.001$.

linewidths.[52] Glu quantification appears to be highly susceptible to linewidth broadening[53] and therefore, narrow linewidths might particularly benefit ^{1}H-MRS focusing on excitatory neurotransmitter levels. Here, the reported linewidth improvement is ~10% lower compared to the original report of spectral registration effects that showed a linewidth reduction of the residual water peak by 31.7%.[20] This is probably explained by the fact that in the present study, spectral registration was compared to minimal frequency alignment using the unsuppressed water peak of multiple interleaved spectra, whereas in the original report, linewidths were compared before and after spectral registration. Regarding GABA, PRESS sequences have limitations because GABA's signal overlaps with resonances from other metabolites and is therefore difficult to detect. Other techniques allow a more reliable GABA detection, such as the Mescher-Garwood (MEGA) PRESS.[54] Yet, MEGA-PRESS is highly susceptible to frequency drifts[55] and requires VOI sizes of ~$30 \times 30 \times 30\,mm^3$, making it unsuitable for the PAG. Moreover, the CRLBs for GABA of the present study (median absolute: 62.44 institutional units (IU), median relative: 24%) indicate an adequate reliability of the concentration measurement and the detected concentrations lie within the expected range for human brain tissue.[56] A disadvantage of the sequence used here is the prolonged scan duration, which might be particularly challenging for patient cohorts. Advances in MR methodology (e.g., higher field strengths) might allow to achieve similar spectral quality with shorter scan durations. Nevertheless, the presented technique offers new opportunities to investigate PAG function and might translate to other clinically relevant small-sized brain regions prone to physiological noise, such as the hippocampus.

Head motion is a source for frequency and phase errors.[20,21] Because spectral registration corrects for frequency and phase errors,[20] it might be particularly useful in cases of greater head motion. Interestingly, the opposite was observed, that is, the more participants moved during the ^{1}H-MRS scan, the smaller the SNR improvement. Potential reasons for this observation were examined by exploring how spectral quality improvement and head motion were associated with measured frequency drifts (displayed in Figure S5) and phase errors. It was observed that (1) spectral registration mainly improved SNR for spectra with larger frequency fluctuations, but not phase fluctuations; and (2) larger phase fluctuations were associated with smaller FWHM NAA improvement (Figure S6). Therefore, in the present study, spectral registration corrected for frequency errors, whereas phase errors impeded effective spectral registration. Head motion did not correlate with frequency drifts or phase errors, but previous studies have shown that translational head motion leads to phase shifts, whereas frequency changes in response to small head movements may be negligible.[21] Taken together, head motion might have induced phase errors that spectral registration was not able to account for, resulting in negative effects on spectral quality improvement. Of note, the motion tracking system used here is based on 3D surface tracking, which cannot be directly translated to the actual displacement of the PAG. Therefore, it is possible that smaller scale motion (e.g., physiological motion of the brainstem) was corrected for by spectral registration. Overall, the markerless motion tracking system allows simple real-time head motion monitoring, which might help decisions on whether a sequence should be repeated because of excessive head motion.

TABLE 1 Quality measures and metabolite concentrations for ^{1}H-MRS spectra acquired in the periaqueductal gray.

Measure	With spectral registration	Without spectral registration	Difference	Difference [%]	*Z*	*p*	Effect size *r*
SNR	18.0 (17.00 to 20.00)	18.0 (16.00 to 19.75)	1.0 (0.00 to 1.00)	4.8 (0.00 to 6.25)	2.26	0.026	0.41
FWHM NAA [Hz]	4.3 (3.96 to 4.85)	5.9 (4.85 to 6.90)	−1.2 (−1.92 to 0.90)	−22.6 (−29.63 to 14.81)	−4.72	<0.001	0.86
CRLB tCr [IU]	22.6 (21.78 to 24.50)	23.0 (22.08 to 30.80)	−0.3 (−0.67 to 0.12)	−1.3 (−3.10 to 0.57)	−2.22	0.026	0.41
CRLB tCho [IU]	9.9 (7.72 to 10.93)	10.7 (9.38 to 11.85)	−0.2 (−0.92 to 0.09)	−2.5 (−7.5 to −0.89)	−3.96	<0.001	0.72
CRLB tmI [IU]	38.0 (31.33 to 41.37)	39.9 (34.72 to 43.05)	−0.4 (−1.03 to −0.14)	−1.3 (−2.82 to −0.43)	−2.49	0.017	0.45
CRLB tNAA [IU]	29.5 (28.42 to 30.60)	30.0 (28.54 to 32.11)	−0.4 (−0.62 to 0.08)	−1.3 (−2.10 to 0.24)	−2.72	0.013	0.50
CRLB Glx [IU]	83.6 (77.84 to 89.25)	85.5 (81.34 to 94.10)	−4.1 (−6.62 to 0.32)	−4.7 (−6.83 to 0.37)	−2.53	0.017	0.46
CRLB GABA [IU]	62.44 (52.29 to 66.35)	72.47 (64.11 to 77.51)	−10.4 (−14.00 to 3.93)	−14.7 (−19.18 to 6.50)	−4.77	<0.001	0.87
CRLB tCr [%]	2 (2–2)	2 (2–3)					
CRLB tCho [%]	3 (2–3)	3 (3–3)					
CRLB tmI [%]	3 (2–3)	3 (3–3)					
CRLB tNAA [%]	2 (2–2)	2 (2–2)					
CRLB Glx [%]	5 (5–6)	5 (5–6)					
CRLB GABA [%]	24 (20–27)	21.5 (17.25 to 28.75)					
	WR-shortTR water signal	WR-longTR water signal					
tCreCr [mmol/kg]	6.2 (6.05 to 6.45)	6.7 (6.42 to 6.93)	0.5 (0.36 to 0.61)	7.5 (5.75 to 9.21)[a]	4.35	<0.001	0.79
tCho [mmol/kg]	2.1 (1.93 to 2.18)	2.2 (2.08 to 2.35)	0.2 (0.12 to 0.20)	7.5 (5.75 to 9.21)[a]	4.35	<0.001	0.79
tmI [mmol/kg]	7.7 (7.14 to 8.07)	8.2 (7.74 to 8.64)	0.6 (0.45 to 0.74)	7.5 (5.75 to 9.21)[a]	4.31	<0.001	0.79
tNAA [mmol/kg]	8.3 (8.15 to 8.56)	8.9 (8.56 to 9.44)	0.6 (0.47 to 0.76)	7.5 (5.75 to 9.21)[a]	4.39	<0.001	0.80
Glx [mmol/kg]	9.2 (8.49 to 10.13)	9.7 (9.06 to 10.73)	0.7 (0.52 to 0.89)	7.5 (5.75 to 9.21)[a]	4.29	<0.001	0.78
GABA [mmol/kg]	1.5 (1.26 to 1.67)	1.6 (1.33 to 1.83)	0.1 (0.06 to 0.15)	7.5 (5.75 to 9.21)[a]	4.41	<0.001	0.81

Note: Quality measures are reported for spectra with spectral registration and without spectral registration. Values are reported as median (interquartile range). Relative CRLBs are provided to help with interpretability, but were not compared between the two postprocessing approaches because they are dependent on metabolite concentrations.[41] Absolute CRLBs were calculated by multiplying the relative CRLBs with the metabolite concentration as ratio to water from the LCModel output. Metabolite concentrations are reported for the metabolite quantification approach using the WR-shortTR water signal and the WR-longTR water signal. Relative differences in % were calculated as difference (with spectral registration – without spectral registration and WR-longTR – WR-shortTR) divided by the baseline value, that is, quality measures of spectra processed without spectral registration or metabolite concentrations using the WR-shortTR water signal, respectively. Statistical comparisons were made using Pratt signed-rank tests.[42] *p*-values were false discovery rate corrected for n = 8 tests (quality measures comparison) or n = 6 tests (metabolite concentration comparison). Effect size interpretation: 0.1 to <0.3; medium effect: 0.3 to <0.5; large effect: ≥0.5.[43]

Abbreviations: CRLB, Cramér-Rao lower bound; GABA, γ-aminobutyric acid; Glx, glutamate + glutamine; IU, institutional units; tCho, glycerophosphocholine + phosphocholine; tCr, Cr + phosphocreatine; tmI, myo-inositol + glycine; tNAA, NAA + N-acetylaspartylglutamate.

[a]The relative difference was identical for all metabolites because it was driven by differently estimated water signals that affected all metabolites to the same degree.

The current gold standard for metabolite quantification is referencing the metabolite signal to the water signal from the same VOI corrected for partial volume and tissue-specific relaxation effects.[57] Literature provides reference values for the required tissue-specific water T_1/T_2 relaxation times, but these might not generalize to the PAG because T_1/T_2 relaxation times vary across different brain regions.[30–32] Therefore, metabolite concentrations were not only quantified using literature-based (WR-shortTR), but also individual-based (WR-longTR) water relaxation times. Using the individual-based approach, 7.5% higher metabolite concentrations were estimated compared to the literature-based approach, meaning that the estimated water signal was smaller when individual-based water relaxation times were used. This effect is most likely because of T_1 relaxation time differences between the two approaches, because the literature-based T_2 relaxation times used here were similar to the T_2 values estimated via the TE series in the WR-longTR scan. This result raises the question whether the standard T_1 relaxation times apply to the PAG. Regardless, the "absolute" metabolite concentrations reported are valuable in that they allow comparison to future PAG ^{1}H-MRS studies.

In summary, spectral registration enabled the acquisition of high-quality ^{1}H-MR spectra in the PAG, a physiologically and clinically highly relevant brainstem region. This approach offers the opportunity to further investigate the PAG's neurochemical properties in health and disease and might not only be applicable in the PAG, but in other brain regions with similar methodological challenges.

ACKNOWLEDGMENTS

This study was funded by the Clinical Research Priority Program "Pain" of the University of Zurich. L.S. is supported by the Theodor und Ida Herzog-Egli Stiftung. We express our gratitude to Emma Louise Kessler, MD for her generous donation to the Zurich Institute of Forensic Medicine, University of Zurich, Switzerland. We thank all participants who took part in the study. Additionally, we thank Lucas Tauschek, Simon Carisch, Madeleine Hau, and Alexandros Guekos for their support during data acquisition. Open access funding provided by University of Zurich.

DATA AVAILABILITY STATEMENT

Data will be made available on request for participants who gave informed consent on further use of their anonymized data.

ORCID

Laura Sirucek https://orcid.org/0000-0001-5599-3546

TWITTER

Laura Sirucek LauraSirucek

REFERENCES

1. Benarroch EE. Periaqueductal gray: an interface for behavioral control. *Neurology*. 2012;78:210-217.
2. Zhou J, Greicius MD, Gennatas ED, et al. Divergent network connectivity changes in behavioural variant frontotemporal dementia and Alzheimer's disease. *Brain*. 2010;133:1352-1367.
3. Cole LJ, Gavrilescu M, Johnston LA, et al. The impact of Alzheimer's disease on the functional connectivity between brain regions underlying pain perception. *Eur J Pain*. 2011;15:568.e1-11.
4. Mainero C, Boshyan J, Hadjikhani N. Altered functional magnetic resonance imaging resting-state connectivity in periaqueductal gray networks in migraine. *Ann Neurol*. 2011;70:838-845.
5. Li Z, Liu M, Lan L, et al. Altered periaqueductal gray resting state functional connectivity in migraine and the modulation effect of treatment. *Sci Rep*. 2016;6:20298.
6. Niu X, Bai L, Sun Y, et al. Disruption of periaqueductal grey-default mode network functional connectivity predicts persistent post-traumatic headache in mild traumatic brain injury. *J Neurol Neurosurg Psychiatry*. 2019;90:326-332.
7. Cifre I, Sitges C, Fraiman D, et al. Disrupted functional connectivity of the pain network in fibromyalgia. *Psychosom Med*. 2012;74:55-62.
8. Truini A, Tinelli E, Gerardi MC, et al. Abnormal resting state functional connectivity of the periaqueductal grey in patients with fibromyalgia. *Clin Exp Rheumatol*. 2016;34:S129-S133.
9. Harper DE, Ichesco E, Schrepf A, et al. Resting functional connectivity of the periaqueductal gray is associated with Normal inhibition and pathological facilitation in conditioned pain modulation. *J Pain*. 2018;19:635 e1-635 e615.
10. Mills EP, Di Pietro F, Alshelh Z, et al. Brainstem pain-control circuitry connectivity in chronic neuropathic pain. *J Neurosci*. 2018;38:465-473.
11. Yu R, Gollub RL, Spaeth R, Napadow V, Wasan A, Kong J. Disrupted functional connectivity of the periaqueductal gray in chronic low back pain. *Neuroimage Clin*. 2014;6:100-108.
12. Lai TH, Fuh JL, Lirng JF, Lin CP, Wang SJ. Brainstem 1H-MR spectroscopy in episodic and chronic migraine. *J Headache Pain*. 2012;13:645-651.
13. Wang W, Zhang X, Bai X, et al. Gamma-aminobutyric acid and glutamate/glutamine levels in the dentate nucleus and periaqueductal gray with episodic and chronic migraine: a proton magnetic resonance spectroscopy study. *J Headache Pain*. 2022;23:83.
14. Buonanotte F, Schurrer C, Carpinella M, et al. Alteration of the antinociceptive systems in chronic daily headaches. *Rev Neurol*. 2006;43:263-267.
15. Serrano-Munoz D, Galan-Arriero I, Avila-Martin G, et al. Deficient inhibitory endogenous pain modulation correlates with periaqueductal gray matter metabolites during chronic whiplash injury. *Clin J Pain*. 2019;35:668-677.
16. Duvernoy HM. *The Human Brain Stem and Cerebellum: Surface, Structure, Vascularization, and Three-Dimensional Sectional Anatomy, with MRI*. Springer Science & Business Media; 1995.

17. Brooks JC, Faull OK, Pattinson KT, Jenkinson M. Physiological noise in brainstem FMRI. *Front Hum Neurosci*. 2013;7:623.
18. Adam A, Dixon AK, Gillard JH. *Grainger & Allison's Diagnostic Radiology: A Textbook of Medical Imaging*. Elsevier; 2020.
19. Edelstein WA, Glover GH, Hardy CJ, Redington RW. The intrinsic signal-to-noise ratio in NMR imaging. *Magn Reson Med*. 1986;3:604-618.
20. Near J, Edden R, Evans CJ, Paquin R, Harris A, Jezzard P. Frequency and phase drift correction of magnetic resonance spectroscopy data by spectral registration in the time domain. *Magn Reson Med*. 2015;73:44-50.
21. Saleh MG, Edden RAE, Chang L, Ernst T. Motion correction in magnetic resonance spectroscopy. *Magn Reson Med*. 2020;84:2312-2326.
22. Bottomley PA. Google Patents, assignee. Selective volume method for performing localized NMR spectroscopy. US Patent 4,480,228. October 30, 1984.
23. Ordidge R, Bendall M, Gordon R, Connelly A. Volume selection for in-vivo biological spectroscopy. *Magnetic Resonance in Biology and Medicine*. 1985;387-397.
24. Edden RA, Schar M, Hillis AE, Barker PB. Optimized detection of lactate at high fields using inner volume saturation. *Magn Reson Med*. 2006;56:912-917.
25. Schulte RF, Henning A, Tsao J, Boesiger P, Pruessmann KP. Design of broadband RF pulses with polynomial-phase response. *J Magn Reson*. 2007;186:167-175.
26. Wilson M, Andronesi O, Barker PB, et al. Methodological consensus on clinical proton MRS of the brain: review and recommendations. *Magn Reson Med*. 2019;82:527-550.
27. Deelchand DK, Kantarci K, Oz G. Improved localization, spectral quality, and repeatability with advanced MRS methodology in the clinical setting. *Magn Reson Med*. 2018;79:1241-1250.
28. Oz G, Deelchand DK, Wijnen JP, et al. Advanced single voxel (1) H magnetic resonance spectroscopy techniques in humans: Experts' consensus recommendations. *NMR Biomed*. 2020;34:e4236.
29. Olesen OV, Wilm J, Kouwe AV, et al. An MRI Compatible Surface Scanner. In Proceedings of the 22nd Annual Meeting of ISMRM, Milan, Italy. 2014 Abstract 1303.
30. Wright PJ, Mougin OE, Totman JJ, et al. Water proton T1 measurements in brain tissue at 7, 3, and 1.5 T using IR-EPI, IR-TSE, and MPRAGE: results and optimization. *Magma*. 2008;21:121-130.
31. Mejia AF, Sweeney EM, Dewey B, et al. Statistical estimation of T1 relaxation times using conventional magnetic resonance imaging. *Neuroimage*. 2016;133:176-188.
32. Thaler C, Hartramph I, Stellmann JP, et al. T1 relaxation times in the cortex and thalamus are associated with working memory and information processing speed in patients with multiple sclerosis. *Front Neurol*. 2021;12:789812.
33. Simpson R, Devenyi GA, Jezzard P, Hennessy TJ, Near J. Advanced processing and simulation of MRS data using the FID appliance (FID-A)-an open source. *MATLAB-Based Toolkit Magn Reson Med*. 2017;77:23-33.
34. Klose U. In vivo proton spectroscopy in presence of eddy currents. *Magn Reson Med*. 1990;14:26-30.
35. Leys C, Ley C, Klein O, Bernard P, Licata L. Detecting outliers: do not use standard deviation around the mean, use absolute deviation around the median. *J Exp Soc Psychol*. 2013;49:764-766.
36. Provencher SW. Estimation of metabolite concentrations from localized in vivo proton NMR spectra. *Magn Reson Med*. 1993;30:672-679.
37. Kreis R, Ernst T, Ross BD. Absolute quantitation of water and metabolites in the human brain. *II Metabolite Concentrations Journal of Magnetic Resonance, Series B*. 1993;102:9-19.
38. Olesen OV, Sullivan JM, Mulnix T, et al. List-mode PET motion correction using markerless head tracking: proof-of-concept with scans of human subject. *IEEE Trans Med Imaging*. 2013;32:200-209.
39. Slipsager JM, Ellegaard AH, Glimberg SL, et al. Markerless motion tracking and correction for PET, MRI, and simultaneous PET/MRI. *PloS One*. 2019;14:e0215524.
40. Benjaminsen C, Jensen RR, Wighton P, et al. *Real Time MRI Motion Correction with Markerless Tracking*. Proceedings of the 24th Annual Meeting of ISMRM; 2016 (abstract 1860).
41. Kreis R. The trouble with quality filtering based on relative Cramer-Rao lower bounds. *Magn Reson Med*. 2016;75:15-18.
42. Pratt JW. Remarks on zeros and ties in the Wilcoxon signed rank procedures. *J Am Stat Assoc*. 1959;54:655-667.
43. Cohen J. A power primer. *Psychol Bull*. 1992;112:155-159.
44. Oz G, Hutter D, Tkac I, et al. Neurochemical alterations in spinocerebellar ataxia type 1 and their correlations with clinical status. *Mov Disord*. 2010;25:1253-1261.
45. Oz G, Tkac I. Short-echo, single-shot, full-intensity proton magnetic resonance spectroscopy for neurochemical profiling at 4 T: validation in the cerebellum and brainstem. *Magn Reson Med*. 2011;65:901-910.
46. Deelchand DK, Adanyeguh IM, Emir UE, et al. Two-site reproducibility of cerebellar and brainstem neurochemical profiles with short-echo, single-voxel MRS at 3T. *Magn Reson Med*. 2015;73:1718-1725.
47. de Matos NMP, Hock A, Wyss M, Ettlin DA, Brugger M. Neurochemical dynamics of acute orofacial pain in the human trigeminal brainstem nuclear complex. *Neuroimage*. 2017;162:162-172.
48. Younis S, Hougaard A, Christensen CE, et al. Effects of sildenafil and calcitonin gene-related peptide on brainstem glutamate levels: a pharmacological proton magnetic resonance spectroscopy study at 3.0 T. *J Headache Pain*. 2018;19:44.
49. Younis S, Hougaard A, Christensen CE, et al. Interictal pontine metabolism in migraine without aura patients: a 3 tesla proton magnetic resonance spectroscopy study. *Neuroimage Clin*. 2021;32:102824.
50. Emir UE, Tuite PJ, Oz G. Elevated pontine and putamenal GABA levels in mild-moderate Parkinson disease detected by 7 tesla proton MRS. *PloS One*. 2012;7:e30918.
51. Bartha R. Effect of signal-to-noise ratio and spectral linewidth on metabolite quantification at 4 T. *NMR Biomed*. 2007;20:512-521.
52. Geurts JJ, Barkhof F, Castelijns JA, et al. Quantitative 1H-MRS of healthy human cortex, hippocampus, and thalamus: metabolite concentrations, quantification precision, and reproducibility. *J Magn Reson Imaging*. 2004;20:366-371.
53. Zhang Y, Shen J. Effects of noise and linewidth on in vivo analysis of glutamate at 3 T. *J Magn Reson*. 2020;314:106732.
54. Mescher M, Merkle H, Kirsch J, Garwood M, Gruetter R. Simultaneous in vivo spectral editing and water suppression. *NMR Biomed*. 1998;11:266-272.
55. Harris AD, Glaubitz B, Near J, et al. Impact of frequency drift on gamma-aminobutyric acid-edited MR spectroscopy. *Magn Reson Med*. 2014;72:941-948.

56. Govindaraju V, Young K, Maudsley AA. Proton NMR chemical shifts and coupling constants for brain metabolites. *NMR Biomed*. 2000;13:129-153.
57. Near J, Harris AD, Juchem C, et al. Preprocessing, analysis and quantification in single-voxel magnetic resonance spectroscopy: experts' consensus recommendations. *NMR Biomed*. 2021;34:e4257.
58. Mikkelsen M, Barker PB, Bhattacharyya PK, et al. Big GABA: edited MR spectroscopy at 24 research sites. *Neuroimage*. 2017;159:32-45.

SUPPORTING INFORMATION

Additional supporting information may be found in the online version of the article at the publisher's website.

Figure S1. Details on the markeless motion tracking system Tracoline TCL3 (TracInnovations, Ballerup, Denmark). The Tracoline is a 3D stereo vision system, which uses structured invisible infrared light to construct 3D point clouds of the participant's face. (A) The set-up of the Tracoline system. (B) A 3D point cloud reconstruction example (for participant anonymity purposes of author LS's face). The TracSuite software estimates head motion by setting a reference point cloud to which subsequent point clouds are registered to. The calculated 3D motion represents the absolute motion of the point cloud's centroid point. (C) Schematic representation (left panel) and mathematical description (right panel) of how 3D motion relates to the conventional six-parameter description of head motion, that is, x-, y-, and z- translations and rotations. 3D motion reflects the length of the translation vector between the point cloud centroid point at its starting position T_0 and the point cloud centroid point at T_1. The schematic contains only translations because rotations cannot be accurately illustrated in this type of schematic.

Figure S2. Excluded ^{1}H-MR spectra acquired in the brainstem periaqueductal gray. Based on visual inspection for artifacts, the same three spectra were excluded for spectra processed with spectral registration and spectra processed without spectral registration, that is, minimal frequency alignment using interleaved unsuppressed water peaks.

Figure S3. Less improvement in spectral quality with greater head motion. Because the majority of investigated outcome measures was not normally distributed, a Spearman's correlation was performed on the ranks of the relative SNR differences (Δ; SNR with spectral registration—SNR without spectral registration divided by SNR without spectral registration; positive values reflecting an SNR improvement using spectral registration) and mean head displacement (3D DIFF) (A). To help with interpretability, the raw data is shown in (B).

Figure S4. Higher metabolite concentrations using individual-based water relaxation times. Differences (Δ) in metabolite concentration estimates were calculated by subtracting the values obtained with literature-based water relaxation times from the values obtained with individual-based water relaxation times. Positive differences reflect higher metabolite concentrations individual-based water relaxation times. $***p < 0.001$. GABA: γ-aminobutyric acid; Glx: glutamate + glutamine; tCho: glycerophosphocholine + phosphocholine; tCr: Cr + phosphocreatine; tmI: myo-inositol + glycine; tNAA: NAA + N-acetylaspartylglutamate.

Figure S5. Frequency drift as determined with spectral registration shown for all measured subjects over the whole ^{1}H-MRS acquisition. To allow comparison with previous reports of frequency drifts on Philips MR systems (e.g.,[58]) the values obtained in Hz were converted to ppm (− value in [Hz] / 127 + 4.68). The observed overall frequency drifts are comparable to previously published data,[58] except for larger subject-specific variations that were most likely because of the smaller volume of interest size used in the present study. The dashed line represents the nominal water frequency (4.68 ppm).

Figure S6. Associations of spectral quality improvement with frequency drifts and phase errors. Standard deviations (SD) of measured frequencies and phases served as measure of frequency and phase fluctuations, respectively. (A) Association of SNR improvement with frequency fluctuations. (B) No association of SNR improvement with phase fluctuations. (C) Association of FWHM of the NAA peak (FWHM NAA) improvement with phase fluctuations. Relative differences (Δ): value with spectral registration—value without spectral registration divided by value without spectral registration. An improvement using spectral registration is reflected in positive Δ for SNR and in negative Δ for FWHM NAA. Because the majority of investigated outcome measures was not normally distributed, Spearman's correlations were performed. Left panels show the ranked data and, to help with interpretability, the raw data is shown in the right panels. Multiple comparison correction was not performed because of the exploratory nature of this analysis.

Table S1. Technical details of the ^{1}H-MRS acquisition using the experts' consensus checklist for a single voxel ^{1}H-MRS study.

How to cite this article: Sirucek L, Zoelch N, Schweinhardt P. Improving magnetic resonance spectroscopy in the brainstem periaqueductal gray using spectral registration. *Magn Reson Med*. 2024;91:28-38. doi: 10.1002/mrm.29832